Liquefaction of second-layer ^{4}He films on graphite*

Samuel E. Polanco† and Michael Bretz
Department of Physics, University of Michigan, Ann Arbor, Michigan 48109
(Received 23 August 1977)

We present the heat capacity of partial second-layer ^{4}He films adsorbed on Grafoil below 2 K. The second-layer liquefaction temperature occurs near 0.75 K which is substantially less than the 1.3 K observed for monolayer liquefaction. This rescaling in T is thought to result from a vertical spread in the wave functions and hence a reduced Van der Waals interaction between adsorbed helium atoms. A consistent picture emerges when the total heat-capacity signals are modified by compressible-monolayer and film-heterogeneity considerations. The resulting liquefaction phase diagram clearly indicates a critical point near 0.025/Å^2 and some altered higher-coverage behavior.

I. INTRODUCTION

There is growing evidence that the specific-heat peak observed is dilute monolayers of ^{4}He adsorbed on Grafoil[1,2] is caused by evaporation of a two-dimensional (2D) liquid.[3,4] This liquid-gas transition is first seen at a temperature of 1.25 K for an areal density $n = 0.027$ atoms/Å.^{2} With increasing coverage the peak broadens and shifts toward higher temperatures, but cannot be followed past $n \sim 0.05$ because the film becomes a 2D solid epitaxial with the substrate. A search for similar second-layer liquefaction disclosed, surprisingly, a shift in the temperature of the maximum to well below 1 K, the temperature limit of that study.[5] The present paper is an extended specific-heat investigation using the actual Grafoil cell A of Refs. 1 and 5, but placed in a ^{3}He cryostat capable of reaching 0.3 K. A preliminary report along with that for the comparable ^{3}He system has been published previously.[6,7]

Our experimental and data-reduction procedures are outlined in Sec. II and III, respectively. The fully reduced data are presented in Sec. IV, where we also give a discussion on results, interpretations, and possible future directions.

II. EXPERIMENTAL PROCEDURES, ADSORPTION ISOTHERM, AND ERROR DISCUSSION

Details of cell-A construction have already been published[1] and will not be repeated here, other than mentioning that it consisted of a oxygen-free high-conductivity thin-walled copper cylinder filled with Grafoil disks. The cell was protected with an atmosphere of argon during shipment from Seattle and installation in the present ^{3}He cryostat. It was attached below the ^{3}He pot by a 4-cm-long 1.3-cm-o.d. cylinder of 0.13-mm-thick Mylar which allowed for good thermal isolation while providing a low vibration support for the cell. The 0.83-mm-i.d. stainless fill line to the cell was isolated from the helium bath by a vacuum jacket above the 1-K pot. A 0.76-mm-diam gold wire was flattened, then wrapped around and varnished to the cell. Contact with the ^{3}He pot was made via a bellows-type heat switch that was activated at 60 psi of helium gas. The gas handling manifold was monitored by a Baratron capacitive manometer with 1000- and 1-Torr heads.[8] Volume calibration to 0.3% was made by expansion of helium gas from a calibrated glass bulb. Helium gas was admitted to the manifold from the bath and metered into the calorimeter through a small cold trap.

Temperatures were measured by a 56-Ω Allen-Bradley and a 100-Ω Speer $\frac{1}{2}$-W carbon resistor mounted with copper-loaded Apiezon-N grease to holes in the top of the cell. A standard wheatstone bridge fed a phase-sensitive detector which was constructed in house.[9] Thermometer resistances R were converted to temperatures by fitting the calibration data for $1/T$ with a seventh-order orthogonal polynomial in $\ln(R)$. The 380-Ω Evanohm heater wire was isolated from its surroundings by superconducting leads with a four-terminal hookup which allowed precise measurement of electrical power at the cell. Heater times were measured with a HP5245L frequency counter and scaler which was activated by double-throw mercury-wetted relays. These relays simultaneously switched the cell heat circuit to a 18-V dc supply. Before and after heating, resistance drifts were fitted with straight lines and extrapolated to the center of the heating interval. Raw data reduction was performed on a HP65 calculator which provided immediate values of temperature T, heat-temperature increment ΔT, empty-calorimeter heat capacity $C_E(T)$, and total heat capacity $C(T)$. $C_E(T)$ was approximated with a straight line in $\ln(C)$ vs $\ln(T)$ and subtracted from C.[10] Data were taken below 2 K since a previous study with this cell[5] found that layer promotion

and desorption heat-capacity contributions[11] occur only at higher temperatures. These corrections are negligible in the present analysis.

A 4.18-K ^{4}He vapor-pressure isotherm taken in the present cryostat is shown in Fig. 1. It matches the previous ^{4}He isotherm of Ref. 1 in all respects except for an offset of 3 cm^3 STP. After carefully rechecking our calibrations, we can only conclude that there has been a slight increase in the heterogeneous surface area. Helium atoms probably cluster in the vicinity of these impurities before subsequent adsorbed helium atoms begin plating the bare basal planes of graphite. Thus, the monolayer completion is taken as 99.5 cm^3 STP rather than the 96.5 cm^3 STP of Ref. 1. This is augmented with the low-pressure data of Stewart, Siegel, and Goodstein obtained with a residual-gas analyzer.[12] Coverage normalization between the two sets of data was accomplished by requiring a smooth merger in the pressure range 10^{-2}–10^{-1} Torr. Since Stewart *et al.* had originally calibrated indirectly to the cell-A monolayer heat-capacity peaks the present shift was only a few percent. $\mathrm{Log}_{10}(P)$ is plotted in Fig. 1 to provide a linear scale (top) for the chemical potential μ which is related to the pressure P through the ideal gas relation[13]

$$\mu = kT \ln(P\lambda^3/kT) \ .$$

Here λ is the thermal de Broglie wavelength and k is Boltzmann's constant. The entire adsorbed system (monolayer, multilayers, and vapor phase) is at the same chemical potential when in equilibrium, so adsorbed gas N vs μ is a more fundamental plot than the traditional N-vs-P isotherm which emphasizes the vapor phase.

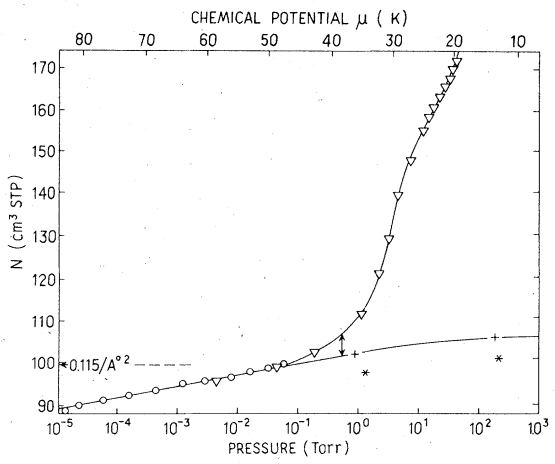

FIG. 1. Pressure (lower scale) and chemical potential (upper scale) plotted vs quantity of adsorbed gas N giving isotherm at 4.18 K. (▽) Data from this run, (○) normalized data of Stewart, Siegel, and Goodstein, (*) neutron-scattering data, (+) our normalization of that data. Solid lines represent our proposed chemical potential for the underlying monolayer and total adsorption isotherm. Horizontal arrow gives monolayer areal density. Vertical arrow refers to example in text.

It should be noted that the calculated second-layer specific heat is far more sensitive to measurement errors and analysis assumptions than the partial monolayer. This is because the monolayer coverage N_1 is quite large and must be subtracted from the total coverage N to obtain (in the present case) a small second layer coverage N_2 which is then divided into C to obtain the specific heat. Owing to these uncertainties in measurement, and also in our knowledge of microcrystallite size effects, first-second layer interactions, inhomogeneities, and geometry of Grafoil, etc., a precise treatment of the second-layer data is not possible at this time. However, a *consistent* and therefore valuable picture of second-layer film behavior does emerge from the various data-reduction possibilities.

III. RESULTS AND ANALYSIS

A. Inert monolayer

The completed ^{4}He monolayer film is a triangular-packed 2D solid with a characteristic Debye temperature of about 56 K.[1] The heat-capacity contribution of this highly compressed solid is quite small in relation to the second-layer signals which we observed below 2 K. The region of completion of the first layer has been investigated by heat-capacity[1] and NMR[14] techniques. Both find a signal minimum at monolayer completion. The raw data of this study were reduced initially by assuming that the underlying monolayer was inert and incompressible, with the coverage fixed at 99.5 cm^3 STP, where the heat-capacity minimum

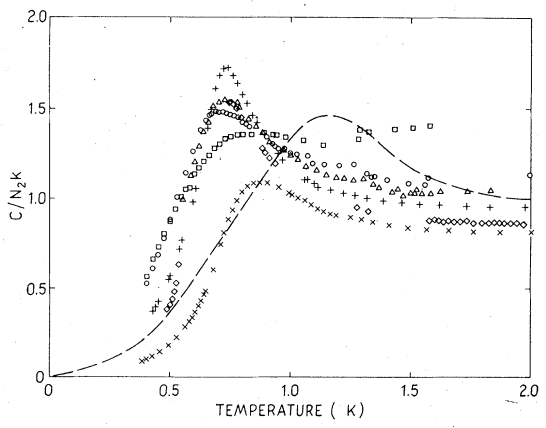

FIG. 2. Raw specific heat. A 99.5-cm^3-STP inert monolayer with $\Theta_D = 56$ K was merely subtracted from the total signal. □, $N = 106.4$; ○, 110.5; △, 113.0; +, 117.6; ◇, 125.0; ×, 135.7 cm^3 STP. Dashed line is a monolayer liquefaction peak near 38 cm^3 STP (Ref. 1).

versus coverage occurred for cell A (normalized from 96.5STPcc reported in Ref. 1). Figure 2 presents our reduced heat-capacity data for the second-layer ^{4}He films using these assumptions. The monolayer signal for $N_1 = 99.5$ cm^3 STP and $\Theta_D = 56$ K was merely subtracted from the data before dividing by $(N - N_1)k$ to obtain C/N_2k, where N_1 and N_2 are the number of atoms in the first and second layers, N is the total number of atoms, and k is Boltzmann's constant.

It is immediately apparent from Fig. 2 that the peaks for partial second-layer films have been suppressed considerably in temperature from those found for equivalent monolayer coverages (dashed line in Fig. 2). (A discussion of 2D liquefaction and this depression in T_c will be deferred until Sec. IV.) The 2-K specific heat for the various films is suggestive of $C/Nk = 1$ for a 2D ideal gas. But there is a substantial variation with coverage, the specific heat dropping markedly as the second layer builds. The behavior is similar to that for the partial monolayer and it is tempting to accept Fig. 2 as the fully reduced results. But we *know* that some poor assumptions were made in this analysis as discussed in Sec. III B.

B. Compressible monolayer

Stewart *et al.*[12] observed a linear dependence of μ with N below monolayer completion. From thermodynamic arguments they obtained the variation of spreading pressure and compressibility of the 2D solid monolayer film with coverage. They concluded that the monolayer is quite compressible and that this compressibility is insensitive to temperature variations. There also exists experimental evidence for monolayer compressibility under our second-layer system. The temperature of the melting peak T_m continues to rise as the monolayer completes and further layers are adsorbed.[1] Since Θ_D is known to vary as $T_m^{1/2}$, the monolayer is active.[15] Carneiro *et al.*[16] have measured the actual monolayer-close-pack interparticle spacings with neutron scattering at 1.2 K where multilayer adsorption was present. They find that the monolayer does indeed compress with overlayer adsorption. Their calibration leads to monolayer areal densities comparable to ours (0.113/Å^2, in Fig. 1). We note that isotherm determinations of monolayer completion are only good to several percent. By changing the coverages of the neutron points in a manner consistent with the uncertainties we can provide a meaningful normalization on the N-vs-μ isotherm of Fig. 1. We choose a normalization such that the neutron-scattering points lay along a smooth extension of the monolayer solid curve[17] (+ in Fig. 1). In this picture, the 2D solid ^{4}He compresses toward monolayer completion, continues compressing as second-layer atoms are added, but tends to level out so that by the third layer and above the monolayer compresses only slightly with added helium. The extended monolayer chemical potential isotherm gives the number of atoms in the first layer N_1. The number of second-layer atoms N_2 for a given total adsorption N can now be determined easily by merely subtracting the extended monolayer chemical potential isotherm from the total curve: $N_2 = N - N_1$. Also, the heat-capacity contribution of the underlying dynamic monolayer of N_1 atoms can be readily determined from $C/k = 28.8(T/\Theta_D)^2 N_1$ for the coverages whose heat capacities were shown in Fig. 1. For example, $N = 106.4$ cm^3 STP yields N_1 of 101.8 cm^3 STP and N_2 of 4.6 as shown by the vertical double-headed arrow in Fig. 1. The Debye temperature is determined from the value of N_1 and a previously published plot of Θ_D vs N.[1]

The full analysis was performed for other extrapolations of the monolayer chemical potential curve but since they leave our qualitative analysis and subsequent phase diagram unchanged, they are not included in Sec. IV. Although taking account of the dynamic monolayer is a somewhat more complicated procedure than merely subtracting the inert monolayer, it is far more satisfying for use in a "consistent picture" of film behavior.

C. Inhomogeneities at low coverages

The resulting heat capacities were recalculated as prescribed above and then plotted as C vs N_2 at several temperatures in Fig. 3. The curves are linear

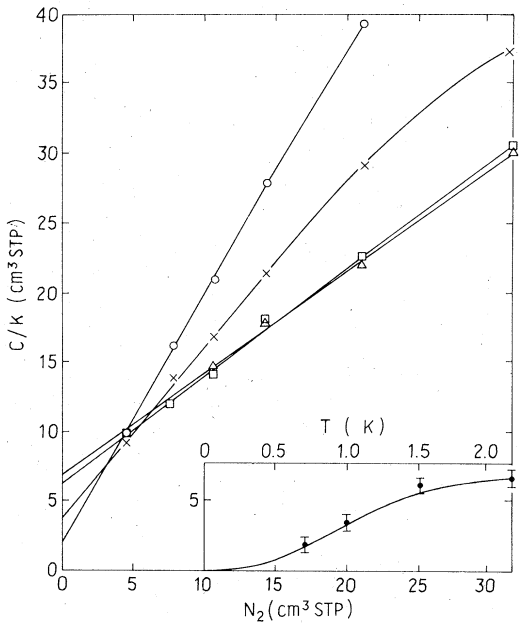

FIG. 3. Ratio of total heat capacity to k (units of cm^3 STP) plotted vs N_2 as determined from Fig. 2. ○: 0.75 K; ×: 1.0 K; □ : 1.5 K; Δ, 2.0 K. Inset: straight-line fit intercepts are plotted vs T. The solid curve is a 2D Debye solid of $\Theta_D = 6.2$ K.

at low and intermediate coverages and thus can be extrapolated to zero coverage. It is significant that the curves do not pass through the origin. There still remains a residual heat-capacity signal. This annoying feature, which was also observed for low monolayer coverages,[1,15] we attribute to film inhomogeneities. The extra gas contributing to this problem is probably contained in the isotherm renormalization discussed previously. (Novaco[18] analyzed isotherm data in this transition region[19] and concluded that a 3% Grafoil-film heterogeneity exists.) The character of the additional heat-capacity signal can be determined quite accurately. The inset in Fig. 3 plots the heat-capacity intercepts versus temperature. This curve is consistent with a Debye heat capacity with Θ_D of 6.2 K (the inhomogeneity at low monolayer coverage[1] fit a curve with $\Theta_D = 5.5$ K). We make this final subtraction from the heat-capacity data of Fig. 2 and present our completely reduced results in Figs. 4–9.

IV. PRESENTATION AND DISCUSSION OF FULLY REDUCED DATA

Several improvements are apparent when comparing the curves of Fig. 4 with those of Fig. 2. At high temperatures all the films approach a common value. There is no longer the sizable C/Nk dependence with coverage which characterized the raw 2-K data. More significantly, the lowest coverage at $N_2 = 4.6$ cm^3 STP, which appeared in Fig. 2 to resemble some manner of quantum gas for all T, now also exhibits a strong maximum near 0.7 K. The low-coverage monolayer peaks (dashed line in Fig. 2 represents 38 cm^3 STP) are believed to be caused by liquefaction from the nonideal quantum gas.[20,21] One sees that the second-layer peaks are similar in shape but are suppressed quite substantially in temperature. Sander, Bretz, and Cole have explained this reduction in T as due to a vertical spread in the atomic wave functions[22] rising from a

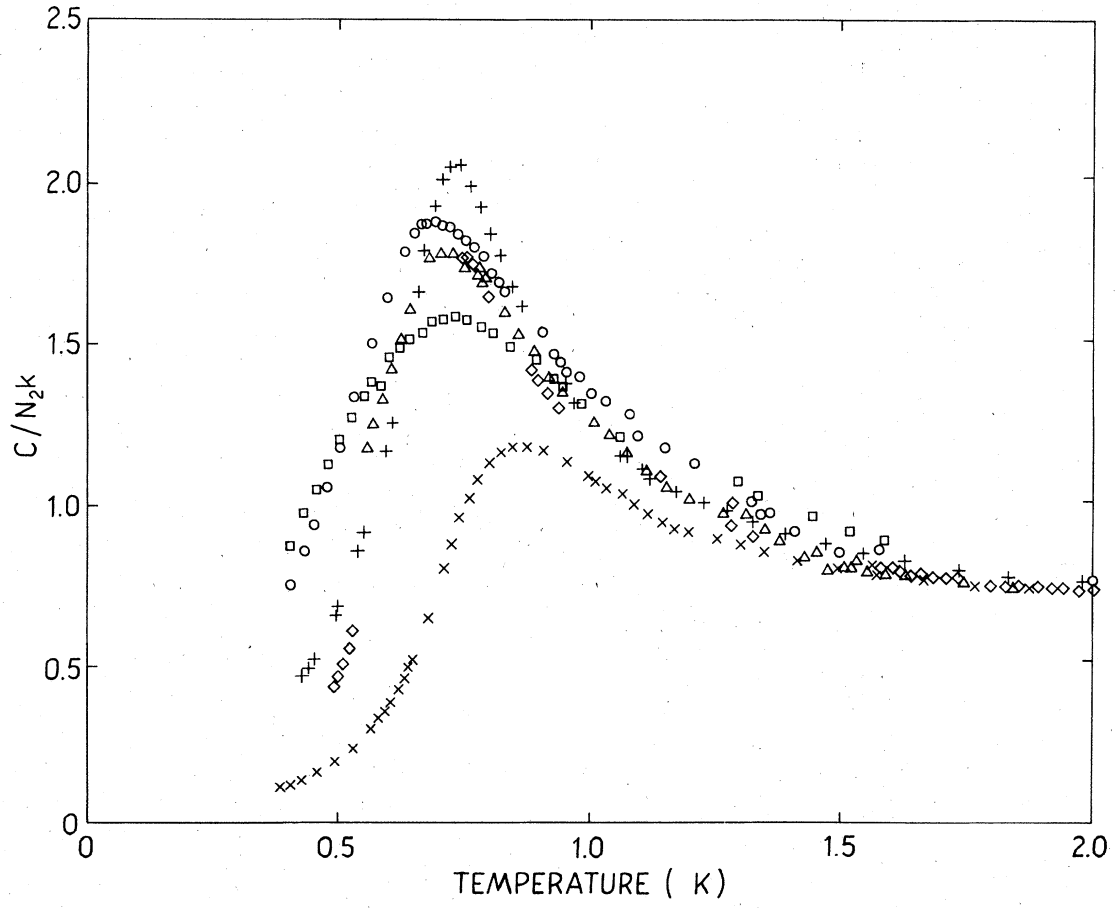

FIG. 4. Fully reduced specific-heat data. □ , $N_2 = 4.6$; ○, 7.8; Δ, 10.7; +, 14.3; □, 21.1; ×, 31.3 cm^3 STP. See Sec. IV.

much lower heat of adsorption than the first layer. A simple Gaussian wave function (and a more-realistic choice by Novaco[23]) led to a reduction in the effective Lennard-Jones parameters, and from the law of corresponding states to the suppressed peak temperatures.

The merger of all the specific heats to about 0.75 near 2 K was a surprise. (Since N_2 is only determined to ± 1 cm^3 STP there must actually be some spread about this value.) We do not understand the origin of the depression of C/Nk below the ideal gas value. Possibly, the second-layer specific heat rises again at higher T where layer promotion and desorption signals are large. The approximate coverage independence points to a particle-substrate interaction rather than interparticle effects. Maybe the altered periodicity of the 2D solid helium substrate restricts the lateral motion of second-layer atoms. Theoretical heat-capacity calculations have already been made for helium adsorbed on periodic surfaces which show high T, coverage independent depressions of specific heat.[24] Surface dimpling[25] or first-second–layer particle exchange[14] might be operative and suppress the specific heat. In any event, there appear to be some interesting theoretical possibilities contained in the data of Fig. 4.

There follow several figures which probe the various aspects of our liquefaction-regime data along with an instructive phase diagram. To explore the low-T features of the heat capacity, we plot $\log_{10}(C/N_2k)$ vs $1/T$ in Fig. 5. The linearity, although not over an extensive range in 1/T, does indicate an exponential heat-capacity behavior. These curves are also consistent with $C/N_2k = A/T^2\exp(-B/T)$, so the precise exponential function cannot be determined. The activation energy for evaporation from the 2D liquid as determined from the slope of Fig. 5 is approximately 0.8 K at 4.6 cm^3 STP. As coverage increases, so does the activation energy which reaches 1.5 K at 14.3 cm^3 STP. This is consistent with the liquefaction peaks at 0.75 K.

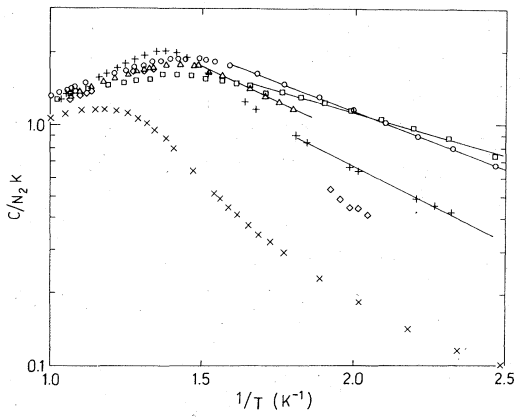

FIG. 5. $\text{Log}_{10}(C/Nk)$ vs $1/T$ indicates the exponential low-temperature behavior. Symbols as in Fig. 4. Solid lines are best eyeball straight-line fits.

We analyze the high-T behavior in Fig. 6. The now standard approach for analysis of specific heats at temperatures above liquefaction is to plot $(C/Nk-1)/n$ vs T, where n is the areal density of the film. This essentially divides out the n dependence of the second virial term in the gas expansion for C/Nk. If higher virial coefficients are negligible then a universal plot should result where $(C/Nk-1)/n$ for all the coverages versus temperature will coincide. In Fig. 6 we have subtracted out the experimental high-T specific heat of 0.75 rather than 1.0 for an ideal 2D gas. One can see universal behavior above about 1.6 K. Error bars for ± 1 cm^3 STP are sufficiently large to account for the divergence of the data at lower T. For comparison, we include the calculation of Siddon and Schick[20] for the specific heat of a quantum virial gas in 2D (solid line in Fig. 6). We conclude that the previously discussed reduction in Lennard-Jones parameters for the second layer has suppressed the universal curve to somewhat lower temperatures than for the monolayer films, which agreed with the Siddon-Schick calculation above 2 K. It should be noted that Van Sciver[7] assumed a single universal curve for second-layer ^{3}He films and determined the N_1 which gave the best agreement for all curves at 1 K.

The temperature and coverage variations of the heat-capacity peaks were carefully investigated by taking data in the peak regions for several additional coverages. These are presented in Fig. 7 using an expanded temperature scale, $0.5 \leq T \leq 1.0$K. The new data were reduced in the manner described in Secs. III B and III C and used in the final plots. Again, uncertainties in N_2 have led to small random variation in the heights of the specific-heat peaks.

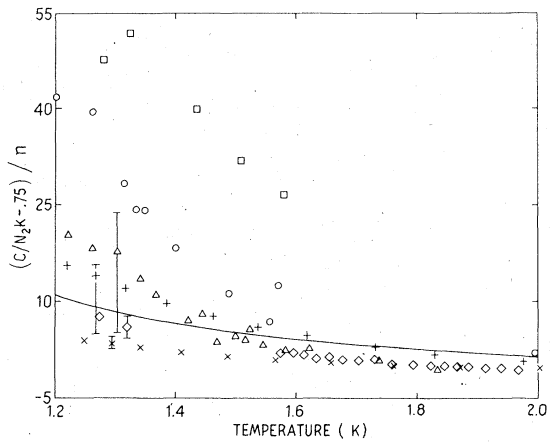

FIG. 6. $(C/N_2k-0.75)/n$ vs T, where the second-layer area is assumed to equal the monolayer area. Solid line is Siddon-Schick estimate for a 2D quantum virial gas. Symbols as in Fig. 4. Error bars reflect ± 1-cm^3-STP uncertainties in N_2.

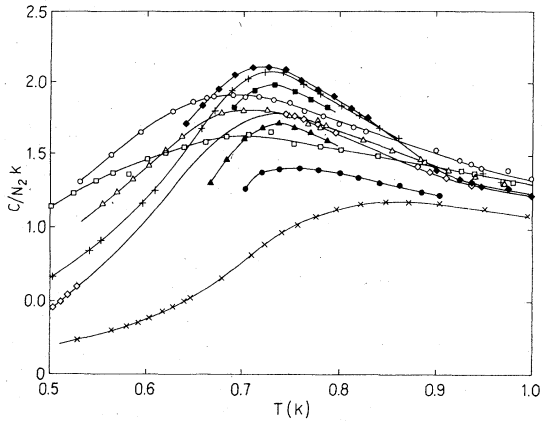

FIG. 7. Specific-heat data for several coverages in the vicinity of the 0.75-K peaks. Symbols as in Fig. 4 and ◆, $N_2 = 12.2$; ■, 16.5; ▲, 19.8; ●, 26.0 cm^3 STP.

The trends of peak height and 2-K total entropy (the fits of Fig. 5 were used for integration) with coverage are given in Fig. 8. For all curves, we observe a linear region for low and moderate N_2. A linear region is expected for the extensive variables C, S in a two-phase system (quasi-2D liquid and gas), and a peak sharpening (see Fig. 4) is consistent with an approach toward the system's critical point. The entropies and peak heights begin to saturate above $N_2 \cong 16$ cm^3 STP and are accompanied by a rapid peak broadening (see Fig. 4) and a dramatic increase of T_p.

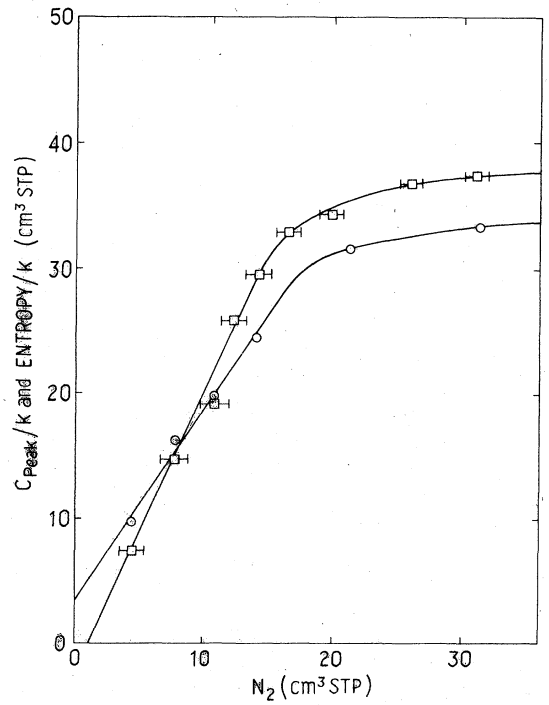

FIG. 8. Plot of peak heights (□) and 2-K entropies (○) vs coverage. Solid lines guide the eye.

Finally a phase diagram is constructed in Fig. 9. The temperatures at peak maximum for each coverage are plotted versus N_2. Vertical error bars represent temperature uncertainties in determining these peak maxima from Fig. 7. Horizontal error bars originate in the determination of N_2 from the isotherm of Fig. 1. Clearly, the phase diagram possesses a curvature. However, we observe that the 4.6-cm^3-STP point occurs at a higher temperature than one would expect from a natural extrapolation of this curvature to 0 K as $N_2 \rightarrow 0$ (solid curve). This can be understood qualitatively as due to regions of slightly greater adsorption energy which encourages liquid puddling. These puddles would be at a higher density than supposed, thus raising the liquefaction temperature. The phase boundary appears to possess a temperature inflection near 20 cm^3 STP and 0.75 K. Near this coverage the specific-heat peaks begin to broaden and increase dramatically in temperature. It seems that by 20 cm^3 STP the 2D liquid puddles have grown sufficiently to cover most of the available surface. At higher coverages evaporation from the liquid causes a sizable increase in the spreading pressure of the 2D vapor, thereby smearing out and increasing the temperature of the transition. Maximum peak height is at about

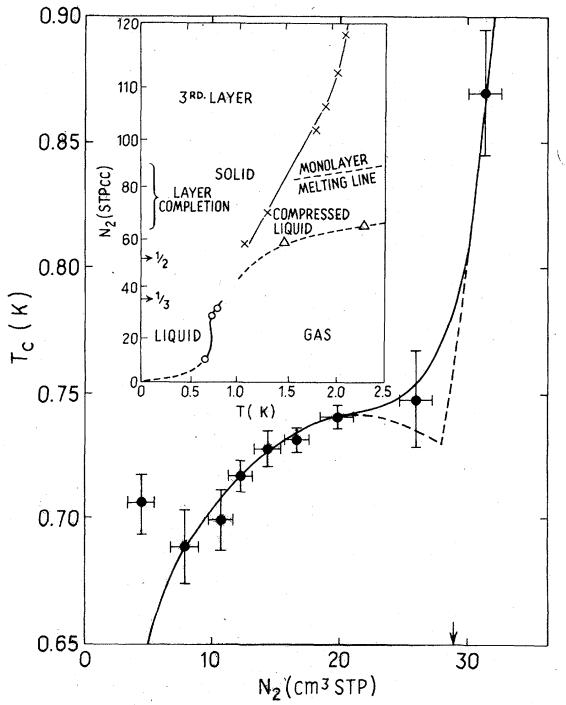

FIG. 9. Phase diagram of the 2D gas-liquid layer. Dashed line suggests one possible shape which has been clouded by heterogeneity and substrate size effects. Arrow denotes liquid density calculated to be (Ref. 21) 0.034/Å^2. Inset gives extended phase diagram with ○, this paper; Δ, broad peaks of Ref. 5; ×, sharp peaks (melting line) of Ref. 5.

16 cm^3 STP and probably critical coverage is in the vicinity of 20–25 cm^3 STP. For comparison we note that Campbell and Schick[21] have calculated semiclassically the binding energy and density of 2D ^{4}He. They estimate that the film should remain self-bound at an energy of −0.61 K per particle and at a density of 0.035 Å^{-2}. Assuming the same area for monolayer and second-layer adsorption, this density translates to a coverage of 29 cm^3 STP for the present system (arrow in Fig. 8) which is reasonably close to the estimated critical coverage. Exact agreement is not expected since theirs is a zero-T calculation and the second-layer atoms possess reduced Lennard-Jones parameters.

The previously reported second-layer data for cell A is above 1 K and showed little peak structure.[5] But at 3.01 and 3.09 layers peaks were seen at 1.5 and 2.5 K which were of uncertain origin. We recalculated N_2 from our Fig. 1 and found that these points fall on an extension of our phase diagram (Δ, Fig. 9 inset) and are similar in shape to the 31.3-cm^3-STP broad peak. The anomalous region, then, appears to extend to quite substantial second-layer coverages. The sharp third-layer peaks of that study are also included in the extended phase diagram (×). They are similar in shape to the monolayer melting peaks[1] and thus were interpreted as second-layer solidification. The monolayer melting line is given by the dotted line in Fig. 9 inset. Our discussion of monolayer compression can be used for the second-layer completion region and third-layer adsorption. The second layer is considerably less dense at layer completion (as determined by a Frankel-Halsey-Hill isotherm[5]) than is the monolayer and so one would expect a substantial compression when the third layer is added. This in turn would lead to an error in third layer coverage determination. We feel that a more accurate placement of the second layer melting line would be toward a merger with the monolayer melting line. Considering that the second-to-first-layer area ratio is unknown and might be as little as 0.9 due to wedge-shaped chambers, etc., we conclude that the second layer probably solidifies as further layers are added. As one extends this melting line to lower coverages, it appears it intersect our low coverage phase diagram just at the anomalous region near 25 cm^3 STP! For this reason we have dotted in a (unresolved) triple point where the 2D gas, solid, and liquid phases appear to merge.

We feel that the phase diagram below N_2 of 8 cm^3 STP and in the region 22–30 cm^3 STP are unresolved due to the inherent small crystallite sizes and uncertain geometry and hetergeneity content of Grafoil. These problems with Grafoil were underscored recently by a heat-capacity study on a different graphite substrate, UCAR-*ZYX*.[2] One of us (M.B.) demonstrated that Grafoil substrate problems limited resolution near the critical region for the $\frac{1}{3}$ ordering transition of monolayer helium films.[26] *ZYX* promises to bypass sizable substrate modification for other film regimes as well. We are presently reinvestigating these unresolved regions on the second-layer phase diagram using this new substrate.

Finally, the positions of possible $\frac{1}{2}$ and $\frac{1}{3}$ ordered solids are indicated by the arrows in the inset of Fig. 9. Since the neutron-scattering results for the helium monolayer[16] find a triangular array, the second-layer wells should form an open hexagonal net leading to an ordered phase at $N_2/N_1 = \frac{1}{2}$. One can see that no data are available between 35 and 59 cm^3 STP so the presence of ordering has not yet been tested.

V. SUMMARY

We have investigated the heat capacity of partial second-layer ^{4}He films adsorbed on Grafoil in the temperature range 0.35–2.0 K. The analysis was not nearly as straightforward as that for the monolayer investigations but we were led to a *consistent* picture of second-layer liquid behavior. We feel that the success of the present picture in itself is further evidence for monolayer compression and that it correctly outlines the shape of the 2D phase diagram. This in turn provides evidence for the existence of a critical point near 20–25 cm^3 STP and an altered high-coverage phase which might be better resolved in the future using more uniform substrates than Grafoil.

ACKNOWLEDGMENTS

We are indebted to J. Magerlein for providing the bridges and phase-sensitive detectors for this experiment and to T. M. Sanders for guidance in construction of the ^{3}He cryostat. Conversations with M. G. Richards and O. E. Vilches were quite helpful.

*Research supported by the NSF Grant No. DMR76-20369.

†Supported in part by The Ford Foundation and a Horace H. Rackham award.

[1]M. Bretz, J. G. Dash, D. C. Hickernell, E. O. McLean, and O. E. Vilches, Phys. Rev. A 8, 1589 (1973).

[2]Grafoil and UCAR oriented graphite grade *ZYX* are products of Union Carbide Crop., Carbon Products Div., 270 Park Ave., New York, N.Y.

[3]A. D. Novaco, J. Low Temp. Phys. 9, 457 (1972).

[4]R. L. Siddon and M. Schick, Phys. Rev. A 9, 1753 (1974).

[5]M. Bretz, in *Monolayer and Submonolayer Helium Films,* edited by J. G. Daunt and E. Lerner (Plenum, New York, 1973).

[6]M. Bretz and S. E. Polanco, *Proceedings of the Fourteenth*

International Conference on Low Temperature Physics, Otaniemi, Finland (North-Holland/Americal Elsevier, Amsterdam, 1975), p. 451.

[7]S. W. Van Sciver, in Ref. 6, p. 368.

[8]MKS Instruments Inc., Burlington, Mass.

[9]G. I. Rochlin, Rev. Sci. Instrum. 41, 73 (1970).

[10]The empty calorimeter heat capacity was consistent with that measured in Seattle and the estimated heat capacity of the attached gold wire.

[11]J. G. Dash, R. E. Peierls, and G. A. Stewart, Phys. Rev. A 2, 932 (1970).

[12]G. A. Stewart, S. Siegel, and D. L. Goodstein, in *Proceedings of the Thirteenth International Conference on Low Temperature Physics,* edited by R. H. Kropschot and K. D. Timmerhaus (Plenum, New York, 1974).

[13]L. D. Landau and E. M. Lifschitz, *Statistical Physics,* 2nd ed. (Addison-Wesley, Reading, Mass., 1969).

[14]B. P. Cowan, M. G. Richards, A. L. Thomson, and W. J. Mullin, Phys. Rev. Lett. 38, 165 (1977).

[15]R. L. Elgin and R. L. Goodstein, Phys. Rev. A 9, 2657 (1974).

[16]K. Carneiro, W. D. Ellenson, L. Passell, J. P. McTague, and H. Taub, Phys. Rev. Lett. 37, 1695 (1976).

[17]The positioning of these points in pressure was determined from the stated filling fraction and the 4-K isotherm. Our renormalization of their data shifts the points in pressure as well as coverage since we are sliding along an isotherm of finite slope.

[18]A. D. Novaco, J. Low Temp. Phys. 21, 359 (1975).

[19]G. J. Goellner, J. G. Daunt, and E. Lerner, J. Low Temp. Phys. 21, 347 (1975).

[20]R. L. Siddon and M. Schick, Phys. Rev. A 9, 907 (1974).

[21]C. E. Campbell and M. Schick, Phys. Rev. A 3, 691 (1971).

[22]L. M. Sander, M. Bretz and M. W. Cole, Phys. Rev. B 14, 61 (1976).

[23]A. D. Novaco, Phys. Rev. B 13, 3194 (1976).

[24]A. D. Novaco and F. J. Milford, Phys. Rev. A 5, 783 (1972).

[25]M. Nielsen and L. Passell (private communication) suggested that the broadening of the neutron-scattering peaks with coverage indicated monolayer dimpling, or depressions in the presence of second-layer atoms. This would result in monolayer compression with a fixed N_1. If so, then motion of the second-layer atom would be hindered by their dimples. We view this compressibility argument as speculative at the present time.

[26]M. Bretz, Phys. Rev. Lett. 38, 501 (1977).